ELECTROMECHANICAL MODELING AND EXPERIMENTAL VALIDATION OF A DUAL-TRANSDUCTION ELECTRODYNAMIC WIRELESS POWER RECEIVER

Miah A. Halim, Spencer E. Smith, Adrian A. Rendon-Hernandez, and David P. Arnold
Interdisciplinary Microsystems Group, University of Florida, Gainesville FL, USA

ABSTRACT

We present the characterization and an experimentally validated electromechanical model of a dual-transduction receiver for an electrodynamic wireless power transmission (EWPT) system. The receiver makes use of both piezoelectric and electrodynamic transducers to generate electrical power simultaneously while operating at its torsion mode mechanical resonance (~744 Hz). The system behavior and output performance under low-frequency, magnetic near-fields are analyzed by establishing an equivalent lumped-element circuit model. A prototype device is fabricated, characterized, and the experimental results are compared with the model predictions under various loading and input conditions. This chip-sized (0.09 cm^3), volume-efficient design offers a low-profile and compact footprint for wearable and implantable medical devices applications.

KEYWORDS

Dual-transduction, electromechanical, piezoelectric, electrodynamic, torsion mode, wireless power transfer.

INTRODUCTION

Electromechanical transducers (e.g., piezoelectric, electromagnetic/electrodynamic, electrostatic etc.) have long been studied as kinetic energy harvesting systems to power or recharge batteries in modern electronic devices including wearable and implantable biomedical devices [1, 2]. Additionally, interest in wireless power transfer (WPT) methods has been growing over the past decade in order to facilitate higher re-charge rates [3, 4]. Compared to conventional high-frequency inductive near-field WPT schemes, electrodynamic (EWPT) (a.k.a. "magneto-mechano-electric") systems leverage low-frequency magnetic fields (<1 kHz) that safely pass through conductive media (e.g., metal, human body etc.) and facilitate wireless power to compact electromechanical receivers [4].

In operation, the low-frequency magnetic field (usually generated by a transmitter coil) mechanically excites a permanent magnet in the EWPT receiver which is then converted to electrical energy via one or more electromechanical transduction schemes among which commonly used transduction schemes are piezoelectric (PE) and electrodynamic (ED) (interaction between permanent magnet and a coil). In order to achieve maximized output performance from an EWPT receiver under any given B-field and to maximize the power transfer efficiency of the EWPT system, it is important to understand the system behavior for which lumped-element modeling is widely used. For instance, design, modeling and experimental validation of EWPT systems using PE [5] and ED [6] receivers have been reported to parameterize the corresponding system and to predict their output performances.

It is well known that PE transducers have higher electrical output impedance and generally produce higher voltage but lower current. ED transducers, on the other hand, have lower output impedance and generate lower voltage and higher current. For the intended applications, higher voltages are desired to facilitate efficient downstream power management circuits, whereas significant power (the product of voltage and current) is required for any practical electronic load application. In order to comply with that, experimental characterization of a dual-transduction EWPT receiver that makes use of both PE and ED transducers simultaneously has recently been reported [7].

This work explores the electromechanical system behavior of the previously reported dual-transduction EWPT receiver while both transducers operate simultaneously. We have developed an equivalent lumped-element model (LEM) of the coupled system to analyze system performance under various loading and input conditions. Finally, the model is validated by experimentally characterizing a fabricated and assembled prototype.

RECEVER DESIGN AND MODELING

Figure 1 illustrates the schematics of the dual-transduction EWPT receiver that comprises an oscillating structure combining both PE and ED transducers. Two piezoelectric elements attached to the clamped arms of a meandering suspension form PE transducer (two piezoelectric unimorphs in series electrical connection). A laterally magnetized square permanent magnet attached to the center platform of the suspension (via spacer) and a rectangular coil fixed to the anchor base that surrounds the magnet (both on the side opposite to the piezoelectric elements) form the ED transducer. The overall dimensions of the EWPT receiver are 7.6 × 7.6 × 1.65 mm^3.

While subjected to an external time-varying magnetic near-fields of desired frequency and amplitude, a torque is induced on the receiver magnet that allows it to oscillate torsionally. As a result, a dynamic stress is generated on the piezoelectric elements which, in turn, generates electricity via direct piezoelectric effect. Simultaneously, the oscillation of the receiver magnet induces an electromotive force (emf) in the receiver coil by means of electrodynamic transduction. In both PE and ED transduc-

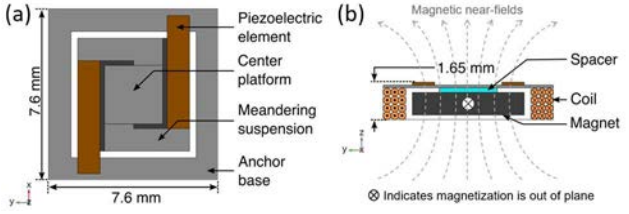

Figure 1: Schematics of the dual-transduction EWPT receiver: (a) top view and (b) cross-sectional view with interacting magnetic near-fields.

tion modes, maximum voltage and power are generated at the torsional resonance of the mechanical suspension with the receiver oriented perpendicular to the incoming magnetic fields.

In order to analyze the system behavior and predict the output performance of the dual-transduction EWPT receiver, a lumped-element equivalent electrical circuit model, represented in Figure 2, is developed. In this model, τ_{mag} is the torque induced on the receiver magnet due to the interacting (along z-axis) magnetic fields B_z, determined as

$$\tau_{mag} = \frac{B_r}{\mu_0} v_{mag} B_z \tag{1}$$

where B_r is the remanence of the magnetic material, μ_0 is the permeability of free space and v_{mag} is the volume of the magnet. The mechanical oscillator is represented by torsional damping coefficient b, mass moment of inertia J and short-circuit torsional spring stiffness k. C_0 represents the clamped electrical capacitance of the PE transducer, R_R represents the coil resistance of the ED transducer, and they both are coupled to the mechanical elements via a transformer of turn ratio Γ_P and a gyrator having ED transduction coefficient K_R, respectively. Finally, the output electrical ports are connected to respective load resistances, R_{L-PE} and R_{L-ED}. Note that the dielectric loss tangent ($tan\delta$) of the piezoelectric material and inductance of the receiver coil have negligible influence on the system performance and hence, are neglected in the model.

According to the fundamentals of electromechanical transduction principle and the electrical and mechanical equations of equilibrium [8, 9]

$$k = (1 - \kappa^2) k_0 \tag{2}$$

$$C_0 = (1 - \kappa^2) C \tag{3}$$

$$\Gamma_P = \sqrt{\kappa^2 k C} \tag{4}$$

$$K_R = \frac{V_{ED}}{\dot{\theta}} \tag{5}$$

where $\kappa^2 = 1 - (f_{r-sc}/f_{r-oc})^2$ is the electromechanical coupling factor determined from the short-circuit f_{r-sc} and open-circuit f_{r-oc} resonant frequencies, $k_0 = J(2\pi f_{r-oc})^2$ is the open-circuit torsional spring stiffness, $C = C_p/2$ represents the free electrical capacitance of two series connected identical piezoelectric unimorphs of capacitance C_p and $\dot{\theta}$ is the angular velocity of the receiver magnet

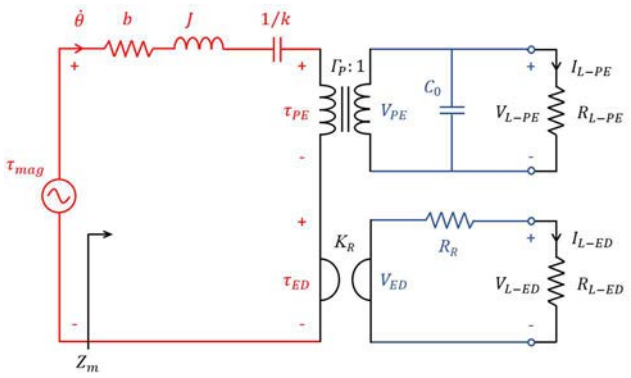

Figure 2: Lumped-element equivalent electrical circuit representation of the dual-transduction EWPT receiver with resistive loads.

while operating. Using standard ac circuit analysis, the frequency-dependent voltages simultaneously generated across the load resistances for the PE and ED transducers are, respectively

$$V_{L-PE} = \frac{\tau_{mag}\Gamma_P R_{L-PE}}{(1+j\omega C_0 R_{L-PE})\left[\left(b+j\omega J+\frac{k}{j\omega}\right)+\frac{\Gamma_P^2 R_{L-PE}}{1+j\omega C_0 R_{L-PE}}+\frac{K_R^2}{R_R+R_{L-ED}}\right]} \tag{6}$$

$$V_{L-ED} = \frac{\tau_{mag}K_R R_{L-ED}}{(R_R+R_{L-ED})\left[\left(b+j\omega J+\frac{k}{j\omega}\right)+\frac{\Gamma_P^2 R_{L-PE}}{1+j\omega C_0 R_{L-PE}}+\frac{K_R^2}{R_R+R_{L-ED}}\right]} \tag{7}$$

Here, the term in the square bracket represents the mechanical impedance Z_m of the system. Using root-mean-square (rms) values for τ_{mag} and V_L, corresponding time-average powers are

$$P_{PE} = \frac{V_{L-PE}^2}{R_{L-PE}} \quad \text{and} \quad P_{ED} = \frac{V_{L-ED}^2}{R_{L-ED}} \tag{8}$$

We consider four specific cases to describe the system behavior of the receiver under various harmonic excitation and load conditions:

Case I: PE open-circuit with ED open. When there is no external load connected to the ED transducer, the frequency-dependent no-load (open-circuit) voltage for PE transducer is

$$V_{PE-I} = \frac{\tau_{mag}\Gamma_P}{j\omega C_0\left[\left(b+j\omega J+\frac{k}{j\omega}\right)+\frac{\Gamma_P^2}{j\omega C_0}\right]} \tag{9}$$

Case II: PE open-circuit with ED short. When the ED transducer is short-circuited, the frequency-dependent no-load voltage for PE transducer is

$$V_{PE-II} = \frac{\tau_{mag}\Gamma_P}{j\omega C_0\left[\left(b+j\omega J+\frac{k}{j\omega}\right)+\frac{\Gamma_P^2}{j\omega C_0}+\frac{K_R^2}{R_R}\right]} \tag{10}$$

Case III: ED open-circuit with PE open. With the PE transducer open-circuited, the frequency-dependent no-load voltage for ED transducer is

$$V_{ED-III} = \frac{\tau_{mag}K_R}{\left(b+j\omega J+\frac{k}{j\omega}\right)+\frac{\Gamma_P^2}{j\omega C_0}} \tag{11}$$

Case IV: ED open-circuit with PE short. With the PE transducer short-circuited, the frequency-dependent no-load voltage for ED transducer is

$$V_{ED-IV} = \frac{\tau_{mag}K_R}{\left(b+j\omega J+\frac{k}{j\omega}\right)} \tag{12}$$

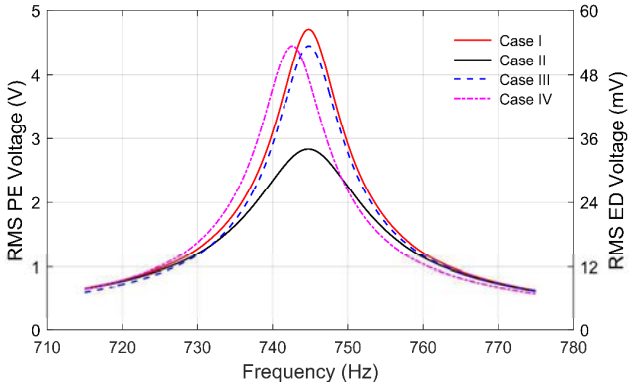

Figure 3: Simulated no-load voltages vs. frequency under 50 μT_{rms} B-field obtained simultaneously from PE (solid lines) and ED (dashed lines) transducers of the receiver.

Table 1: System parameters used for analytical simulation.

Parameter	Value
B_r	1.26 T
v_{mag}	$5 \times 5 \times 1$ mm^3
$^*b$	2.58×10^{-8} N.m.s.rad^{-1}
$^\dagger J$	4.96×10^{-10} Kg.m^2
$^{**}k_0$	1.09×10^{-2} N.m.rad^{-1}
C	313.7 pF
κ^2	5.9×10^{-3}
Γ_P	1.41×10^{-7} N·m·V^{-1}
K_R	1.1×10^{-3} V.s.rad^{-1}
R_R	71 Ω

Determined from *measured mechanical Q-factor ($Q = 90$), **measured f_{r-oc} and †COMSOL finite element simulation

Figure 3 shows the simulated frequency responses of the receiver for the four cases discussed above. Results indicate that the resonant frequencies (f_{r-oc}) for the first three cases are 744.8 Hz whereas that (f_{r-sc}) for Case IV is 742.6 Hz. The ED transducer loading conditions do not have any effect on the PE transducer resonant frequency but affects the PE no-load voltage, depending on the equivalent ED transducer impedance/resistance. The parameters used in the analytical simulation, derived from the geometry and material properties of the receiver components, are summarized in Table 1.

RESULTS AND DISCUSSION

The electromechanical model developed for the dual-transduction EWPT receiver has been verified by experimentally characterizing (using a 28 cm diameter, 15 cm long, 0.74 mT/A Helmholtz coil pair) a fabricated prototype. The suspension structure (1 mm wide) with a center platform (2.6×2.6 mm^2) and surrounding base was formed by laser micro-machining 125 µm thick titanium (Ti) shim stock. A 200 µm-thick silicon spacer (2.6×2.6 mm^2) and a laterally magnetized N50 NdFeB magnet were bonded to one side of the center platform using cyanoacrylate. A self-supported, rectangular shaped (5.6×5.6×1.4 mm^3) copper coil (44 AWG, 328 turns) was glued to the surrounding base. Two PZT-5A (Piezo Systems, USA) piezo-ceramic patches (5×1×0.13 mm^3) with sputtered nickel electrodes, poled through the thickness were bonded to the clamped arms of the suspen sion using electrically conductive epoxy (EO-21M-5, Epoxy Set Inc., USA) in a series electrical configuration. Finally, the structure was assembled on a printed circuit board (PCB) and electrical connections were created for measurements (figure 4a).

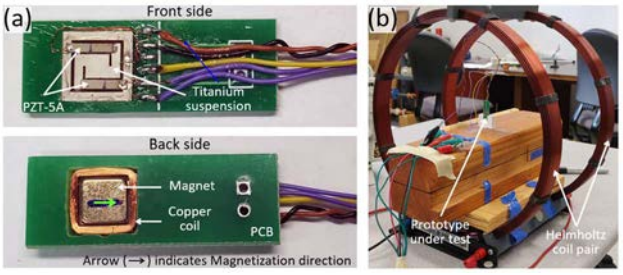

Figure 4: Photographs of (a) a fabricated prototype and (b) the experimental setup with Helmholtz coil pair.

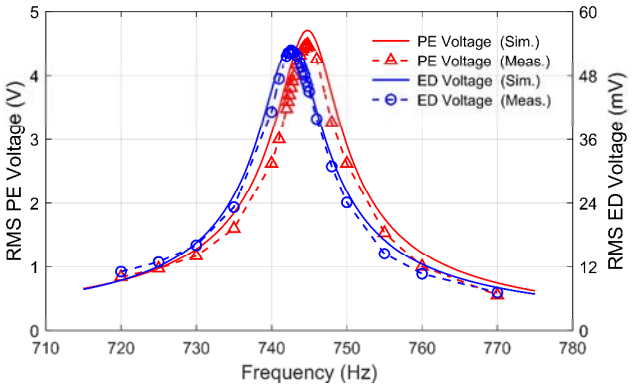

Figure 5: Simulated and measured PE voltage with ED open (Case I) and ED voltage with PE short (Case IV), under 50 µT$_{rms}$ B-field.

The assembled prototype was placed at the centroid of the Helmholtz coil pair (figure 4b) and the initial tests were done under 50 µT$_{rms}$ B-field. Figure 5 shows no-load voltages as a function of frequency for *Case I* (PE voltage with ED open-circuit) and *Case IV* (ED voltage with PE short-circuit) for which the torsional resonant frequencies are 744.8 Hz (open-circuit) and 742.6 Hz (short-circuit), respectively. Results shows good agreement between simulation (Sim.) and measurement (Meas.), both exhibit linear characteristics with peaks at resonance, indicating an underdamped 2nd-order system with Q-factor of 90 (in air).

In order to determine the optimum load resistances for both transducers, a load sweep was performed on each transducer by connecting a variable load resistance across their outputs for the cases described earlier (figure 5). Each sweep was performed at the resonant frequency of each respective case and under 50 µT$_{rms}$ B-field. Figure 6 shows how the PE load voltage and power changes with load resistance while the ED port was left open-circuited. Both simulation and measurement results show the PE transducer had 600 kΩ optimum load resistance to which the maximum power (8.7 µW) was delivered. Similarly, figure 7 shows the ED load voltage and power vs. load resistance while the PE port was short-circuited. In this case, the measured optimum load resistance is 160 Ω (maximum power 5.8 µW) whereas the simulation predicts 120 Ω. Once we found the optimum load resistance for each transducer, the new resonant frequency was determined as 744.6 Hz by another frequency sweep while

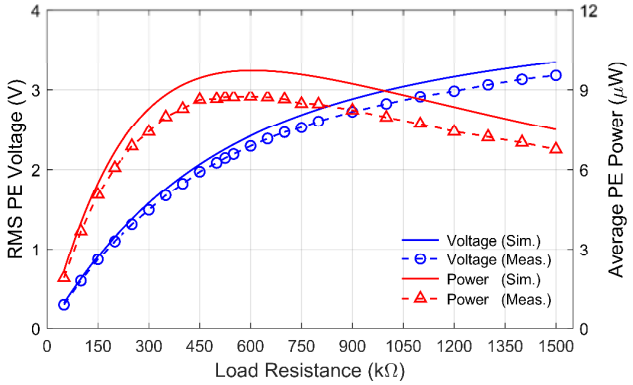

Figure 6: PE load voltage and power (with ED open) vs. load resistance under 50 µT$_{rms}$ B-field at 744.8 Hz resonant frequency (noted as open-circuit resonance, f_{r-oc}).

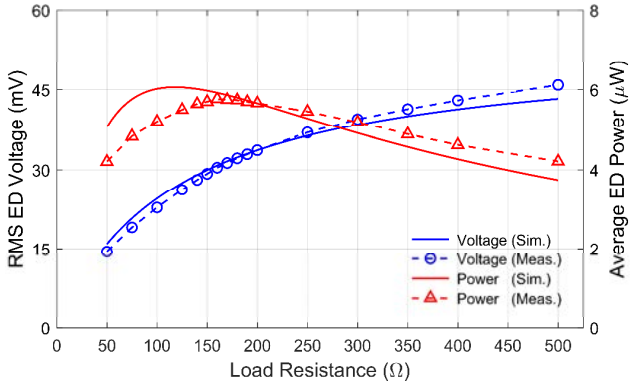

Figure 7: ED load voltage and power (with PE short) vs. load resistance under 50 μT_{rms} B-field at 742.6 Hz resonant frequency (noted as short-circuit resonance, $f_{r\text{-}sc}$).

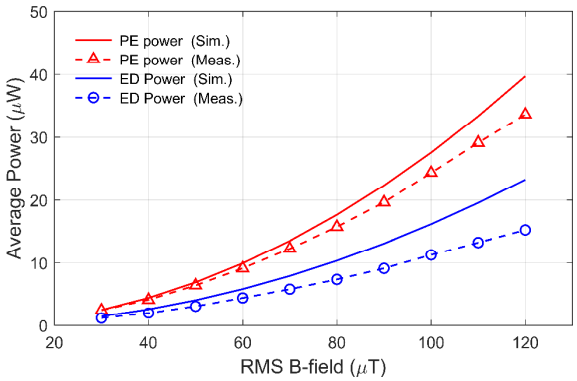

Figure 8: Simultaneously generated power vs. B-field from both PE and ED transducers at 744.6 Hz resonant frequency.

both transducers were connected to the corresponding optimum load resistances.

Finally, the average power simultaneously delivered to the corresponding optimal load resistances of both PE and ED transducer were measured by varying the amplitude of the B-field at 744.6 Hz, as shown in figure 8. Both simulation and measurement show that the power increases quadratically as the magnetic field amplitude increases. However, the measured power values tend to reduce as the field intensity increases which show the nonlinear behavior of the system. Potential reasons of this nonlinearity include mechanical spring stiffening effect at higher field amplitudes, nonlinear piezoelectric properties for the PE transducer, and change of K_R value with change of B-field (as the angular displacement changes) for the ED transducer which was kept constant in the simulation.

CONCLUSION

In this work, we have demonstrated a dual-transduction EWPT receiver for low-frequency, near-field wireless power transfer systems by developing an electromechanical lumped-element model, which is then validated by experimental characterization of a fabricated prototype. This dual-transduction receiver simultaneously generates voltage/power from a PE transducer and an ED transducer while operates at its torsional vibration mode by the influence of an external time-varying B-field. From the analyses as well as the experimental characterization, it is observed that the maximum transferable power under a given B-field can be achieved by concurrently tuning the driving frequency and adapting the load resistance for each transducer. Experimental results show good agreement with the model predictions. However, some deviations (24% maximum), especially when the B-field is increased, have been observed due to nonlinearities that require further analysis.

ACKNOWLEDGEMENTS

This work was supported in part by the IoT4Ag Engineering Research Center funded by the National Science Foundation (NSF) under NSF Cooperative Agreement Number EEC-1941529. Any opinions, findings and conclusions, or recommendations expressed in this material are those of the author(s), and do not necessarily reflect those of the NSF.

REFERENCES

[1] J. Siang, M. H. Lim, M. S. Leong, "Review of vibration-based energy harvesting technology: Mechanism and architectural approach", *Int. J. Energy Res.*, vol. 42, pp. 1866-1893, 2018.

[2] T. Ghomian, S. Mehraeen, "Survey of energy scavenging for wearable and implantable devices", *Energy*, vol. 178, pp. 33-49, 2019.

[3] A. Garraud, D. P. Arnold, "Advancements in electrodynamic wireless power transmission", in *Tech. Digest IEEE Sensors Conference*, Orlando, October 30 - November 3, 2016, pp. 82-84.

[4] M. A. Halim, A. A. Rendon-Hernandez, D. P. Arnold, "An electrodynamic wireless power receiver 'Chip' for wearables and bio-implants", in *Tech. Digest IEEE PELS WoW Conference*, Seoul, November 15-19, 2020.

[5] M. A. Halim, A. A. Rendon-Hernandez, S. E. Smith, J. M. Samman, N. Garraud, D. P. Arnold, "Miniature electrodynamic wireless power transmission receiver using a micromachined silicon suspension", *J. Microelectromech. Syst.*, vol. 30, pp. 144-155, 2021.

[6] M. A. Halim, A. A. Rendon-Hernandez, S. E. Smith, D. P. Arnold, "A chip-sized piezoelectric receiver for low-frequency, near-field wireless power transfer: design, modeling and experimental validation", *Smart Mater. Struct.*, vol. 30. p. 045011, 2021.

[7] S. E. Smith, M. A. Halim, A. A. Rendon-Hernandez, D. P. Arnold, "Dual-transduction electromechanical receiver for near-field wireless power transmission", in *Tech. Digest IEEE MEMS Conference*, Online, January 25-29, 2021.

[8] S. D. Senturia, *Microsystem Design*, Kluwer Academic Publishers, 2001.

[9] H. A. C. Tilmans, "Equivalent circuit representation of electromechanical transducers: I. Lumped-parameter systems", *J. Micromech. Microeng.*, vol. 6, pp. 157-176, 1996.

CONTACT

*D.P. Arnold, tel: +1-352-392-4931; darnold@ufl.edu